Received: 19 December 2023 | Revised: 13 June 2024 | Accepted: 23 September 2024 | Published online: 29 September 2024

RESEARCH ARTICLE

Journal of Optics and Photonics Research
2025, Vol. 2(4) 191–202
DOI: 10.47852/bonviewJOPR42022330

BON VIEW PUBLISHING

Role of Higher-Order Scattering Coefficient and Residual Nonlinearities on Instability Criteria in Three-Body Bose-Einstein Condensates

P. Mohanraj[1,*], R. Sivakumar[2], Jayaprakash Kaliyamurthy[1], V. Kamalakar[1] and J. Gajendiran[1]

[1]*Department of Physics, Vel Tech Rangarajan Dr. Sagunthala R&D Institute of Science and Technology, India*

[2]*Department of Physics, Pondicherry University, India*

Abstract: We examine the instability characteristics in a three-body condensate and the effect of higher-order nonlinear effects caused by shape-dependent imprisonment and higher-order scattering coefficients such as S-wave scattering length and effective range for collisions. Using the linear stability technique, we study the spreading relations and gain profile of the adapted Gross–Pitaevskii equation with higher-order scattering coefficients and enduring nonlinearity. The role of higher-order interactions S-wave scattering length, residual nonlinearity, and effective range for collisions over the modulational instability in immiscible and miscible three-body Bose-Einstein condensates has been discussed in detail. Modulational instability (MI) can be excited in miscible condensates and changed in immiscible condensates because of residual nonlinearity, without taking into account higher-order nonlinearity and three-body condensates. However, the results of this work demonstrate that the influence of higher-order residual nonlinearity can cause the MI to change in both immiscible and immiscible condensates. The discovered MI spectrum reveals a new soliton production regime in three-body condensates. The results exhibit that higher-order scattering coefficient and remaining nonlinearity interplay can successfully switch the instability gain profile in miscible and immiscible condensates. This makes it possible to regulate the dynamics by varying the MI in a ternary combination of Bose-Einstein condensates.

Keywords: dual-component interactions, instability spectrum, higher-order residual nonlinearity, three-body Bose-Einstein condensate, modified Gross–Pitaevskii equations, higher-order scattering coefficient

1. Introduction

A Bose gas may follow the T = 0 formalism in the ultra-cold zone, where the hotness is significantly less than the condensation critical temperature. The nonlinear mean-field Gross–Pitaevskii equation (GPE) with dual-component communication is the foundation for the theoretical Bose-Einstein condensate (BEC) model, which can reproduce and explain most BEC data. In this work, we considered a ternary mixture of BEC. Such a system has three components of the BEC, which means there will be three kinds of interatomic interaction in this mixture of BEC. Therefore, our system has three "condensates wave functions": (BEC1 (ψ_1), BEC2 (ψ_2), and BEC3 (ψ_3)). The higher-order interactions may intensely alter the instability gain profile of multicomponent condensates. Nonetheless, the typical BP approximation loses some of its predictive power when higher-order alterations are included in the scattering dynamics [1]. It becomes crucial to include higher-order corrections in the GP equation in such a situation.

The result of the interatomic relations is a nonlinear expression in the GP equation that is inversely related to the condensate density and the s-wave scattering length [2]. The Feshbach resonance approach [3] can be used to modify the scattering length's sign and strength. This suggests that various experimental tools can be used to limit how intense the contact is. The GP equation assumes the shape of a nonlinear Schrödinger equation with a range of accurate soliton solutions in the one-dimensional (1D) identical limit. Experimentalists simulate this scientifically idyllic situation by radially restricting the condensate in a stretched-out and prorate trap. However, weak axial harmonic trapping that eliminates the system's integrability is frequently present with this quasi-1D shape [4].

It is known that dual-component relations can be characterized by a sprinkling length where the properties of the higher-order connections are minimal at small densities and where the interatomic distances are substantially more significant than the distance scale of atom-atom relations [5]. However, in other studies, the BEC density is relatively high. In particular, a considerable compression of the traps occurs during the formation of BECs on the surface of atomic chips and in atomic waveguides, which increases the densities of BECs [6]. As a result, more than the straightforward GP equation (using only the two-body contact) is required. Consequently, a better atom-atom interaction description is required for the dynamics of the BEC. Due to increased densities and intense confinement, a system like this has three-body interactions and shape-dependent potential. The straightforward GP equation is corrected by higher-order factors in the extension of the phase shifts at small momenta, which are influenced by the effective range, the shape parameter,

***Corresponding author:** P. Mohanraj, Department of Physics, Vel Tech Rangarajan Dr. Sagunthala R&D Institute of Science and Technology, India. Email: drmohanrajp@veltech.edu.in

etc. The higher-order scattering term has been demonstrated to significantly impact the energy levels, chemical potential, and condensate profiles of a harmonically imprisoned BEC as the scattering length approaches zero [7]. Additionally, the trap potential would significantly impact them because the form parameter controls the higher-order interaction. In this instance, examining the dynamics of BECs while considering higher-order connections is essential, particularly in the case of exact resonances [8, 9]. The current study is very different from the form dependency that results from a dual-component association at shorter length scales at greater densities [10]. As a result, there is a chance to consider the three-body interaction, which is crucial in situations of Efimov resonance and higher densities [11]. Additionally, in a near-collapse scenario, three-body exchanges and the nonlocality of the dual-component crashes should be considered [12]. This system might be the best choice to evaluate the relationships between mesoscopic objects and light, to comprehend the fundamental physics, and to forecast potential uses in current research on quantum information dispensation with ultra-cold bosons in optical resonators [13]. The impact of the optical lattice and three-body atomic interactions on solitons in quasi-one-dimensional (1D BEC) has been documented by Golam Ali et al. [14]. The BEC solitons cannot be destabilized by the three-body interaction in this work because of the connecting factor $g_1 << g_2$. Nevertheless, it might be worthwhile to investigate whether the perturbative impact of these communications could be wisely utilized to obtain fresh physical data about the BEC atoms. Raju et al. [15] have reported about the instability of dual BECs striking. Motivated by this research work, we present a simple MI action of the condensate mixture with ternary components. Two GP equations control the dynamics of the ternary components of BEC in a purely growing mode. This article demonstrates how, at appropriate parameter fixings, higher-order communications in ternary-species condensates can be crucial to determining MI criteria in miscible condensates and altering MI criteria in immiscible condensates.

Developing spatial dynamics patterns in nonlinear media is crucial to various physical processes [16–18]. MI is necessary to understand pattern creation in a continuous fiber. Due to the combined effects of dispersion, diffraction, and nonlinearity, instability occurs when a steady-state-wave environment in a spatially nonlinear field becomes unstable to stimulate modified sinusoidal patterns. It is generally known that MI causes a homogeneous medium to fragment into pulsing "solitary waves" [19]. BEC has been developed to be a helpful solution for researching instability and nonlinear matter-wave dynamics. The interaction between the atoms causes the nonlinearity in these systems. Such systems have the advantage that wave matter may be experimentally administered using standard optical, molecular, and atomic physics techniques. The influence of self-interactions in nonlinear media plays a vital role of the instability in a single-component structure, as several studies [20] have highlighted. In our present work, results demonstrate that instability mainly arises in defocusing nonlinearity-based nonlinear media and dual-body condensates [21]. In single-body condensates, the instability leads to several nonlinear excitation processes, including quantized vortices [22], bright solitons [23], dark solitons [24], and others. Several constituent constructions with parameters belonging to more than one order can lead to new types of interactions between various condensate components. The MI of the system as a whole may suffer as a result.

The standard linear stability method and mathematical equation for the instability profile relation are offered in Section 2, the results and discussion, and the miscible and immiscible illustration examination in Section 3, then the Conclusions in Section 4.

2. Mathematical Equation and Standard Linear Stability Method

The following GP equation can be used to represent BEC with three-body and higher-order relations at extremely low temperatures [8, 10, 25]:

$$i\hbar\frac{\partial\Phi[r,t]}{\partial t}=\left[-\frac{\hbar^2}{2m}\nabla^2\Phi[r,t]+V(r)\Phi[r,t]+g|\Phi[r,t]|^2\Phi[r,t]+h|\Phi[r,t]|^4\Phi[r,t]+\eta\nabla^2(|\Phi[r,t]|^2)\Phi[r,t]\right] \tag{1}$$

where m is denoted by the photon's mass and the reduced planks constant is $\hbar$. The coefficients h and g are the interatomic strengths of two and three-body BEC. The parameter g is related to a_s by $g=\frac{4\pi\hbar^2a_s}{m}$. The shape-dependent imprisonment alteration of the dual-component smash potential is described by the final term. The factor η is the higher-order sprinkling factor, which hinges on the effective collision range as well as the s-wave scattering length [25].

According to Kartashov et al. [26], the power of the three-body connection is typically relatively weak compared to the dual contact and depends on the strength of the two-body relationship. However, the three-body interaction can occasionally be dominant and have about the same size and range as the dual-component power [27]. But given the predominance of ternary-component interactions as seen in the case of Efimov resonances [28] and the current prospect of manipulating ternary-component relations independently of dual-component connections, it is imperative to look into how higher-order relationships affect BECs [6].

The focus of this work is on ternary-component condensates, which are characterized by a system of modified classical time-dependent GP equations that are ternary and coupled. First, we begin with the ternary-component condensate governing equations, which incorporate higher-order effective range corrections [18].

$$i\hbar\frac{\partial\psi_1}{\partial t}=\left[-\frac{\hbar^2}{2m}\nabla^2\psi_1+V(r)\psi_1+g_1|\psi_1|^2\psi_1+g_{12}|\psi_2|^2\psi_1+g_{13}|\psi_3|^2\psi_1+h_1|\psi_1|^4\psi_1+h_{12}|\psi_2|^4\psi_1+h_{13}|\psi_3|^4\psi_1+\eta_1\nabla^2(|\psi_1|^2)\psi_1+\eta_{12}\nabla^2(|\psi_2|^2)\psi_1+\eta_{13}\nabla^2(|\psi_3|^2)\psi_1\right] \tag{2}$$

$$i\hbar\frac{\partial\psi_2}{\partial t}=\left[-\frac{\hbar^2}{2m}\nabla^2\psi_2+V(r)\psi_2+g_2|\psi_2|^2\psi_2+g_{21}|\psi_1|^2\psi_2+g_{23}|\psi_3|^2\psi_2+h_2|\psi_2|^4\psi_2+h_{21}|\psi_1|^4\psi_2+h_{23}|\psi_3|^4\psi_2+\eta_2\nabla^2(|\psi_2|^2)\psi_2+\eta_{21}\nabla^2(|\psi_1|^2)\psi_2+\eta_{23}\nabla^2(|\psi_3|^2)\psi_2\right] \tag{3}$$

$$i\hbar\frac{\partial\psi_3}{\partial t}=\left[-\frac{\hbar^2}{2m}\nabla^2\psi_3+V(r)\psi_3+g_3|\psi_3|^2\psi_3+g_{31}|\psi_3|^2\psi_1+g_{32}|\psi_3|^2\psi_2+h_3|\psi_3|^4\psi_3+h_{31}|\psi_3|^4\psi_1+h_{32}|\psi_3|^4\psi_2+\eta_3\nabla^2(|\psi_3|^2)\psi_3+\eta_{31}\nabla^2(|\psi_3|^2)\psi_1+\eta_{32}\nabla^2(|\psi_3|^2)\psi_2\right] \tag{4}$$

The system's ternary distinct components' macroscopic wave functions are denoted as ψ_1, ψ_2 and ψ_3, respectively. Then, g_1, g_2, g_3 take the form for each boson component. The mass would be the decreased mass, as shown below in the equations for inter-component interactions, g_{ij}.

$$g_1 = \frac{4\pi\hbar^2 a_1}{m_1},\ g_2 = \frac{4\pi\hbar^2 a_2}{m_2},\ g_3 = \frac{4\pi\hbar^2 a_3}{m_3},\ g_{12} = \frac{4\pi\hbar^2 a_{12}}{m_{12}},$$
$$g_{13} = \frac{4\pi\hbar^2 a_{13}}{m_{13}}, g_{23} = \frac{4\pi\hbar^2 a_{23}}{m_{23}} \tag{5}$$

where, $a_1, a_2,\ a_3, a_{12}, a_{13},$ and a_{23} are inter and intra-components S-wave sprinkling lengths. Higher-order residual nonlinearity, which takes into consideration the imprisonment caused by the form of condensates, is incorporated into the set of coupled differential Equations (2)–(4). As stated below [10], the effective range of interaction is contained in the residual nonlinearities P_i and P_{ij}.

$$P_1 = g_1\left(\frac{{a_1}^2}{3} - \frac{a_1 r_e}{2}\right),\ P_{12} = g_{12}\left(\frac{{a_{12}}^2}{3} - \frac{a_{12} r_e}{2}\right) \tag{6}$$

To keep things simple, we'll assume that each of the three masses, m_i, is equal. Next, by establishing zero potential, we obtain the active one-dimensional system for the trapless condensates. While non-dimensionalzing, the oscillator length, $\frac{1}{a_\perp}$, and radial frequency, $\frac{1}{\omega_\perp}$, are used to express the timeframe and length scales, respectively. The nonlinearity coefficients in the aforementioned set of equations are

$$g_1 = \frac{2a_1}{a_\perp}, g_2 = \frac{2a_2}{a_\perp}, g_3 = \frac{2a_3}{a_\perp}, g_{21} = \frac{2a_{21}}{a_\perp},\ g_{31} = \frac{2a_{31}}{a_\perp},$$
$$g_{32} = \frac{2a_{32}}{a_\perp},\ P_1 = g_0 g_1,\ P_2 = g_0 g_2,\ P_3 = g_0 g_3, P_{21} = g_0 g_{21}, \tag{7}$$
$$P_{31} = g_0 g_{31}, P_{32} = g_0 g_{32}$$

We consider the interactions to be symmetric in this case, where $g_{ji} = g_{ij}$ and $p_{ji} = p_{ij}$, and the p's and g's stand for the residual nonlinearities and interaction strengths, respectively. The second-order dispersion parameter β is determined by the length scale employed to make the system dimensionless.

In this work, the Laplacian operator represents the second derivative of the concerned wave function ((ψ_1), (ψ_2), and (ψ_3)) with respect to the interatomic length (here considered as "x").

Assume that the trap is turned off, releasing the condensates into free space, and V (x) = 0. As a consequence, the set of equations that follows is dimensionless and appropriate for a standard linear stability examination.

$$i\hbar\frac{\partial\Phi_1}{\partial t} = \Big[-\beta_1\frac{\partial^2\Phi_1}{\partial x^2} + g_1|\Phi_1|^2\Phi_1 + g_{12}|\Phi_2|^2\Phi_1 + g_{13}|\Phi_3|^2\Phi_1$$
$$+ h_1|\Phi_1|^4\Phi_1 + h_{12}|\Phi_2|^4\Phi_1 + h_{13}|\Phi_3|^4\Phi_1 \tag{8}$$
$$+ \eta_1\nabla^2(|\Phi_1|^2)\Phi_1 + \eta_{12}\nabla^2(|\Phi_2|^2)\Phi_1 + \eta_{13}\nabla^2(|\Phi_3|^2)\Phi_1\Big]$$

$$i\hbar\frac{\partial\Phi_2}{\partial t} = \Big[-\beta_2\frac{\partial^2\Phi_2}{\partial x^2} + g_2|\Phi_2|^2\Phi_2 + g_{21}|\Phi_1|^2\Phi_2 + g_{23}|\Phi_3|^2\Phi_2$$
$$+ h_2|\Phi_2|^4\Phi_2 + h_{21}|\Phi_1|^4\Phi_2 + h_{23}|\Phi_3|^4\Phi_2 \tag{9}$$
$$+ \eta_2\nabla^2(|\Phi_2|^2)\Phi_2 + \eta_{21}\nabla^2(|\Phi_1|^2)\Phi_2 + \eta_{23}\nabla^2(|\Phi_3|^2)\Phi_2\Big]$$

$$i\hbar\frac{\partial\Phi_3}{\partial t} = \Big[-\beta_3\frac{\partial^2\Phi_3}{\partial x^2} + g_3|\Phi_3|^2\Phi_3 + g_{31}|\Phi_3|^2\Phi_1 + g_{32}|\Phi_3|^2\Phi_2 + h_3|\Phi_3|^4\Phi_3$$
$$+ h_{31}|\Phi_3|^4\Phi_1 + h_{32}|\Phi_3|^4\Phi_2 + \eta_3\nabla^2(|\Phi_3|^2)\Phi_3$$
$$+ \eta_{31}\nabla^2(|\Phi_3|^2)\Phi_1 + \eta_{32}\nabla^2(|\Phi_3|^2)\Phi_2\Big] \tag{10}$$

2.1. Standard linear stability analysis

Generally, linear stability analysis (LSA) is to perturb the steady-state solution and examine whether the distortion grows or decays with transmission waves. The LSA of the linear-state solution of Equation (11) reveals only the initial exponential growth of weak distortion through the gain. In this study, we are primarily interested in how dual-component interactions affect higher-order residual nonlinearities. Therefore, we take into account the condensate in the trapless environment. As a result, $V(x) = 0$. We then search for the following answers to the fundamental in-plane wave Equations (8)–(10).

$$\phi_1[x,t] = B_1\ \exp[i(k_1 x - \mu_1 t)]$$
$$\phi_2[x,t] = B_2\ \exp[i(k_2 x - \mu_2 t)]$$
$$\phi_3[x,t] = B_3\ \exp[i(k_3 x - \mu_3 t)] \tag{11}$$

Thus, for each of the ternary components, μ's and k's denote the frequency and wave number of the continuous wave backdrop. Equations (8)–(10) can be modified to use the plane wave approach to produce the dispersion relation $\mu\ (k)$.

$$\mu_1 = a_1^2 g_1 + a_2^2 g_{12} + a_3^2 g_{13} + a_1^4 h_1 + a_2^4 h_{12} + a_3^4 h_{13} + k_1^2\beta_1$$
$$\mu_2 = a_2^2 g_2 + a_1^2 g_{21} + a_3^2 g_{23} + a_2^4 h_2 + a_1^4 h_{21} + a_3^4 h_{23} + k_2^2\beta_2$$
$$\mu_3 = a_3^2 g_3 + a_1^2 g_{31} + a_2^2 g_{32} + a_3^4 h_3 + a_1^4 h_{31} + a_2^4 h_{32} + k_3^2\beta_3 \tag{12}$$

Next, we introduce a little perturbation of the type in the Ansatz (Equation (11)).

$$\phi_1[x,t] = (B_1 + \varepsilon_1[x,t])\ \exp[i(k_1 x - \mu_1 t)]$$
$$\phi_2[x,t] = (B_2 + \varepsilon_2[x,t])\ \exp[i(k_2 x - \mu_2 t)]$$
$$\phi_3[x,t] = (B_3 + \varepsilon_3[x,t])\ \exp[i(k_3 x - \mu_3 t)] \tag{13}$$

The dynamical equations for the perturbations can be obtained by linearizing the equations that follow from entering Equation (13) into Equations (8)–(10). These are the real-valued quantities that we specify for convenience.

$$i\frac{\partial\varepsilon_1}{\partial t} + \beta_1\frac{\partial^2\varepsilon_1}{\partial x^2} - a_1^2 g_1(\varepsilon_1 + {\varepsilon_1}^*) - 2a_1^4 h_1(\varepsilon_1 + {\varepsilon_1}^*) - a_1 a_2 g_{12}(\varepsilon_2 + {\varepsilon_2}^*)$$
$$- 2a_1 a_2^3 h_{12}(\varepsilon_2 + {\varepsilon_2}^*) - a_1 a_3 g_{13}(\varepsilon_3 + {\varepsilon_3}^*) - 2a_1 a_3^3 h_{13}(\varepsilon_3 + {\varepsilon_3}^*)$$
$$- a_1^2 P_1\left(\frac{\partial^2\varepsilon_1}{\partial x^2} + \frac{\partial^2{\varepsilon_1}^*}{\partial x^2}\right) - a_1 a_2 P_{12}\left(\frac{\partial^2\varepsilon_2}{\partial x^2} + \frac{\partial^2{\varepsilon_2}^*}{\partial x^2}\right) - a_1 a_3 P_{13}\left(\frac{\partial^2\varepsilon_3}{\partial x^2} + \frac{\partial^2{\varepsilon_3}^*}{\partial x^2}\right) = 0 \tag{14}$$

$$i\frac{\partial\varepsilon_2}{\partial t}+\beta_2\frac{\partial^2\varepsilon_1}{\partial x^2}-a_2^2g_2(\varepsilon_2+\varepsilon_2{}^*)-2a_2^4h_2(\varepsilon_2+\varepsilon_2{}^*)-a_1a_2g_{21}(\varepsilon_1+\varepsilon_1{}^*)$$
$$-2a_1a_2^3h_{21}(\varepsilon_1+\varepsilon_1{}^*)-a_2a_3g_{23}(\varepsilon_3+\varepsilon_3{}^*)-2a_2a_3^3h_{23}(\varepsilon_3+\varepsilon_3{}^*)$$
$$-a_2^2P_2\left(\frac{\partial^2\varepsilon_2}{\partial x^2}+\frac{\partial^2\varepsilon_2{}^*}{\partial x^2}\right)-a_1a_2P_{21}\left(\frac{\partial^2\varepsilon_1}{\partial x^2}+\frac{\partial^2\varepsilon_1{}^*}{\partial x^2}\right)-a_2a_3P_{23}\left(\frac{\partial^2\varepsilon_3}{\partial x^2}+\frac{\partial^2\varepsilon_3{}^*}{\partial x^2}\right)=0 \quad (15)$$

$$i\frac{\partial\varepsilon_3}{\partial t}+\beta_3\frac{\partial^2\varepsilon_2}{\partial x^2}-a_3^2g_3(\varepsilon_3+\varepsilon_3{}^*)-2a_3^4h_3(\varepsilon_3+\varepsilon_3{}^*)-a_1a_3g_{31}(\varepsilon_1+\varepsilon_1{}^*)$$
$$-2a_1a_3^3h_{32}(\varepsilon_2+\varepsilon_2{}^*)-a_2a_3g_{32}(\varepsilon_2+\varepsilon_2{}^*)-2a_2a_3^3h_{32}(\varepsilon_2+\varepsilon_2{}^*)$$
$$-a_3^2P_3\left(\frac{\partial^2\varepsilon_3}{\partial x^2}+\frac{\partial^2\varepsilon_3{}^*}{\partial x^2}\right)-a_3a_2P_{32}\left(\frac{\partial^2\varepsilon_2}{\partial x^2}+\frac{\partial^2\varepsilon_2{}^*}{\partial x^2}\right)-a_1a_3P_{31}\left(\frac{\partial^2\varepsilon_1}{\partial x^2}+\frac{\partial^2\varepsilon_1{}^*}{\partial x^2}\right)=0 \quad (16)$$

Since the aforementioned set of equations for ϵ's is a linearized set, we anticipate continuous wave elucidations in the form shown below and search for conditions that are met.

$$\varepsilon_1[x,t]=u_1\ \exp[i(Qx-\Omega t)]+v_1\ \exp[-i(Qx-\Omega t)]$$
$$\varepsilon_2[x,t]=u_2\ \exp[i(Qx-\Omega t)]+v_2\ \exp[-i(Qx-\Omega t)]$$
$$\varepsilon_3[x,t]=u_3\ \exp[i(Qx-\Omega t)]+v_3\ \exp[-i(Qx-\Omega t)] \quad (17)$$

The perturbation frequency and spatial frequency are represented by the variables Ω and Q, respectively. Six harmonized equations for the agitated amplitudes u's and v's can be obtained by substituting Equations (13)–(15).

$$\begin{pmatrix} M_{11} & M_{12} & M_{13} & M_{14} & M_{15} & M_{16}\\ M_{21} & M_{22} & M_{23} & M_{24} & M_{25} & M_{26}\\ M_{31} & M_{32} & M_{33} & M_{34} & M_{35} & M_{36}\\ M_{41} & M_{42} & M_{43} & M_{44} & M_{45} & M_{46}\\ M_{51} & M_{52} & M_{53} & M_{54} & M_{55} & M_{56}\\ M_{61} & M_{62} & M_{63} & M_{64} & M_{65} & M_{66} \end{pmatrix}\begin{pmatrix} u_1\\ u_2\\ u_3\\ v_1\\ v_2\\ v_3 \end{pmatrix}=0 \quad (18)$$

In the Appendix, a list of every matrix element is provided. If the 6 × 6 determinant created by the coefficients matrix disappears, an arithmetical polynomial with degree six can be found, as stated below, providing a nontrivial solution to the preceding matrix problem.

$$L\Omega^6+\mathrm{M}\Omega^5+\mathrm{N}\Omega^4+\mathrm{O}\Omega^3+\mathrm{P}\Omega^2+\mathrm{Q}\Omega+\mathrm{R}=0 \quad (19)$$

The roots of this polynomial are used to obtain the instability gain by applying the generic expression for the MI gain, which is given by:

$$Gain=\ |Im(\Omega_{\max})| \quad (20)$$

where *Im* represents the imaginary portion of the root and the suffix max indicates the maximum value of the root.

Equation (20) represents the criteria for the occurrence of MI as well as the instability gain. In fact, the system becomes unstable when at least one of the perturbed frequencies acquires an imaginary part. It is therefore sufficient to have $\Omega\pm$ negative for the condensates to undergo MI. The MI gain in this case is expressed in terms of $|Im(\Omega_{max})|$ and depends on the parameters of intra-species (*gj*) and interspecies (*g j*, 4–j) three-body interactions as well as on the strength of intra-species (*pj*) and interspecies (*p j*, 4–j) residual interactions.

Ramakrishnan and Subramaniyan [10] used the standard LSA to investigate the MI gain over two-body condensates with higher-order corrections, such as residual nonlinearity and inter- and intra-species interaction. They demonstrated how the MI was strongly correlated with higher-order residual nonlinearity without trapping potential. In addition, Sabari et al. [17] introduced the variational approach to examine the MI gain over three-body condensates with higher-order correction, including residual nonlinearity and inter- and intra-species interaction. They explained the strong relationship between the effective potential and higher-order residual nonlinearity.

Our current findings diverge from the literature previously mentioned. Because the MI gain spectrum has expanded with slight adjustments to the residual nonlinearity, the stable and unstable regions are heavily influenced by the higher-order inter and intra-species strengths. The novelty of the present work was the MI gain spectrum in three-body condensates without effective potential using LSA, and their results were discussed in detail.

3. MI Dynamical Behavior in Three-Body BEC System

3.1. The g_3–g_{32} parameter plane

We may discover the instability regions and dynamics of the ternary condensate structure by relating the instability gain provided by Equation (20) and the MI condition to Equation (19). We utilize $g_1 = g_2 = g_3$, $h_1 = h_2 = h_3$, $h_{12} = h_{21} = h_{23} = h_{32}$, and similarly for our study's higher-order connections p's. This section displays the MI gain as contour plots, which show both the MI gain's magnitude and its geographic distribution. The analysis would be most effortless when all higher-order outstanding nonlinearities are missing or $p_i = p_{ij} = 0$. In this instance, we display the instability gain on the h_3–g_{32} plane (Figure 1). Such a graph demonstrates the typical immiscible and miscible regions of a three-body system for a three-body BEC. While the other regions contain unstable zones, the unchanging modes can be found in the blue areas. The white dashed lines depict the alteration from an unchanging to an unhinged regime in the parameter plane. The stability region in the plane similarly grows when we raise the strength of h_3. These findings indicate that the instability occurs when the intra-species interaction is repulsive

Figure 1
Modulationally stable and unstable zones in the g_{32}–h_3 plane with other nonlinear parameters. The properties of MI are changed dramatically by g_{32} and h_3

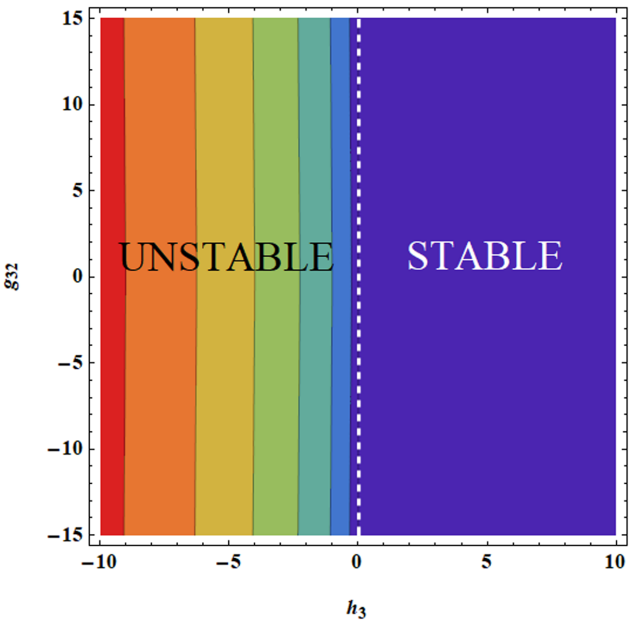

($g_3 > 0$) and the interatomic interaction is attractive ($g_{32} < 0$), thereby satisfying the requirement stated by the white dashed lines. Therefore, the repulsive two-body condensate also exhibits anti-symmetric MI behavior, reversing the sign of the interaction strength in a manner akin to attractive condensates. This indicates that energy excitation beyond the initial perturbation has exchanged symmetry concerning three-body and higher-order interactions governed by the optical potential strength. Additionally, if we disable the higher-order interaction as well, we discover the stability condition as stated in Ramakrishnan and Subramaniyan [10]. Our model exhibits the instability condition reported in Ramakrishnan and Subramaniyan [10] when the three-body interaction is removed. There have been a number of theoretical investigations on how higher-order effects influence the MI in single-component BECs and investigations that take into account three-body interactions [29]. The effects of three-body atomic interaction and optical lattices on solitons in quasi-one-dimensional 1-D BEC were reported by Golam Ali et al. [14]. The BEC solitons cannot be destabilized by the three-body interaction in this study because of the coupling constant $g_1 << g_2$. Nevertheless, it might be worthwhile to investigate whether the perturbative impact of these interactions could be wisely utilized to obtain fresh physical data about the BEC atoms. Raju et al. [15] reported the instability of two BECs colliding. Inspired by this work, we are providing a basic treatment of the MI of the three-species condensate mixture. For the purely growing mode, two GP equations control the three-species BEC dynamics.

A three-component GP equation with higher-order residual nonlinearities describes a ternary mixture of BEC. These interactions are influenced by the shape-dependent confinement of the particles, which has been the subject of our investigation. In the framework of atomic BEC, we outlined the mathematical model and highlighted the physical significance of higher-order nonlinear terms. Next, we determined the system's instability criteria and the rate at which unstable modes were growing using the LSA. This analysis reveals that MI occurs even in miscible three-component condensates, when higher-order shape-dependent interactions are included. Furthermore, the MI in immiscible condensates is strongly modified by the type of higher-order interactions. Ramakrishnan and Subramaniyan [10] have noticed the same type of behavior in two-body condensates. To support their analytical research, the author conducted direct numerical simulations, and the outcomes were found to be in excellent agreement with their analytical predictions. In the scenario where the mixture is expected to be modulationally unstable regardless of immiscibility and non-overlapping chains of bright solitons have been produced. When the unstable mixture is anticipated to be miscible, these solitons are static and thinner in both condensates. If, on the other hand, the unstable mixture is predicted to be immiscible, then the solitons in both condensates are thicker and periodically collide.

A more prosperous MI excitation scenario is achievable in the presence of higher-order connections. Figure 2(a)–(c) depicts the zones of instability for various intensities. The g_3 *vs.* g_{32} plane illustrates the impact of intra-species higher-order interactions (p_3) in particular when $p_{32} = 0$. As observed, the instability region contracts, and stable modes move into the immiscibility region as p_3 increases (assuming positive values signifying intra-species higher-order repulsion). The stability zone widens, admitting more stable methods as well as those with negative g_3 values, as intra-species higher-order communications become supplementary desirable, i.e., when p_3 drops while taking negative values. As a result, stronger intra-species repulsive forces are required to achieve stability with positive p_3 values. Accordingly, the ternary condensate is stabilized by intra-species higher-order attraction, while it is destabilized by intra-species higher-order repulsion. To expand the instability band of three-body condensates, interspecies higher-order relations may be equally as significant as intra-species higher-order communications. When intra-species higher-order collaborations are attractive, the instability zones in the g_3–g_{32} plane for innumerable powers of interspecies higher-order communications are shown in Figure 2(d)–(f). The line $g_{32} = 0$ in the diagram represents the symmetry of the stability region. Similar to $p_{32} = 0$, it denotes the lack of any remaining interspecies interactions. When the inter-component higher-order collaborations are striking, the stability zone moves to lesser values of the inter-component three-body communication. The miscible area swings to larger values of the interspecies three-body relations for revolting inter-component higher-order connections ($p_{32} > 0$). The behavior will be the same whether there are zero ($p_3 = 0$) or repulsive ($p_3 > 0$) intra-species higher-order interactions. As a result, stability is increased when the higher-order and ternary condensate interspecies connections are identical. The conclusions above imply additional requirements for instability and miscibility when higher-order connections are not insignificant. The transfer along the g_{32} axis in Figure 2(d)–(f) is comparable to the shortening of the steadiness area in those figures. Figure 2(a)–(c) shows a shift along the g_3 axis. As a result, the higher-order relations move the MI diagram's position concerning the miscibility illustration in two different directions: to the right for rising p_3 and the left for lowering p_3, and in the other direction for changing p_{32}. Thus, we infer that the miscibility criterion would change to

$$g_1g_2g_3 > g_{12}g_{21} \quad g_1g_2g_3 > g_{23}g_{32} \quad g_1g_2g_3 > g_{13}g_{31} \tag{21}$$

The efficient contact powers have a significant impact on the MI. The wave number reliance would entail a very complex MI cascade situation. The supplementary enthusiastic manners increase the scheme's involvement when second-order MI develops. Effective interactions can improve or change a condensate mixture's immiscibility-miscibility, which can impact the instability excitation. In miscible or phase-mixed states, positive p_3 can, for instance, decrease repulsive three-body interaction and MI excitation. When p_3 and p_{32} are zero, the effective interaction strengths g_3 and g_{32} may change the MI excitation in miscible states. The results obtained by Mithun and Kasamatsu [16] as well as Ramakrishnan and Subramaniyan [10] are completely in line with these findings in terms of quality. The aforementioned findings give us a better understanding of how stable BECs with three-body and higher-order interactions are. Our research should encourage other experimentalists in this direction.

3.2. The h_3–h_{32} parameter plane

In this instance, we display the instability gain on the h_3–g_{32} plane (Figure 3). Such a graph demonstrates the typical miscible and immiscible regions of a three-body system for a three-body BEC. While the other regions contain unbalanced areas, stable modes can be found in the blue areas. The white dashed lines depict the changeover from an unchanging to an unhinged regime in the parameter plane. The stability region in the plane similarly grows when we raise the strength of h_3. This finding indicates that the instability arises when the intra-species collaboration is repellent ($h_3 > 0$) and the interatomic exchange is attracting ($h_{32} < 0$), satisfying the requirement stated by the white dashed lines.

A more prosperous MI excitation scenario is conceivable when higher-order interactions are present. The instability zones for altered intensities of intra-species higher-order connections p_3 in the h_3 *vs.*

Figure 2

Instability domain in the g_3 vs. g_{32} plane with higher-order scattering effect [(a)–(c)] when $h_1 = h_2 = h_3 = 0.5$, $h_{12} = h_{21} = h_{31} = h_{32} = h_{23} = 0$, and $p_{12} = p_{21} = p_{31} = p_{32} = p_{23} = 0$ (no interspecies higher-order interaction) and for numerous powers higher-order intra-species communications $p_3 = 0, 6, -6$; and [(d)–(f)] when $p_3 = -6$ (pretty intra-species higher-order interaction) and for innumerable influences of the interspecies higher-order communication $p_{32} = 0, -3, +3$, respectively. The red regions characterize steady modes, whereas the rest of the area embodies unbalanced modes, with the greatest unbalanced in the black regions. Black dashed lines separate the miscible and immiscible zones

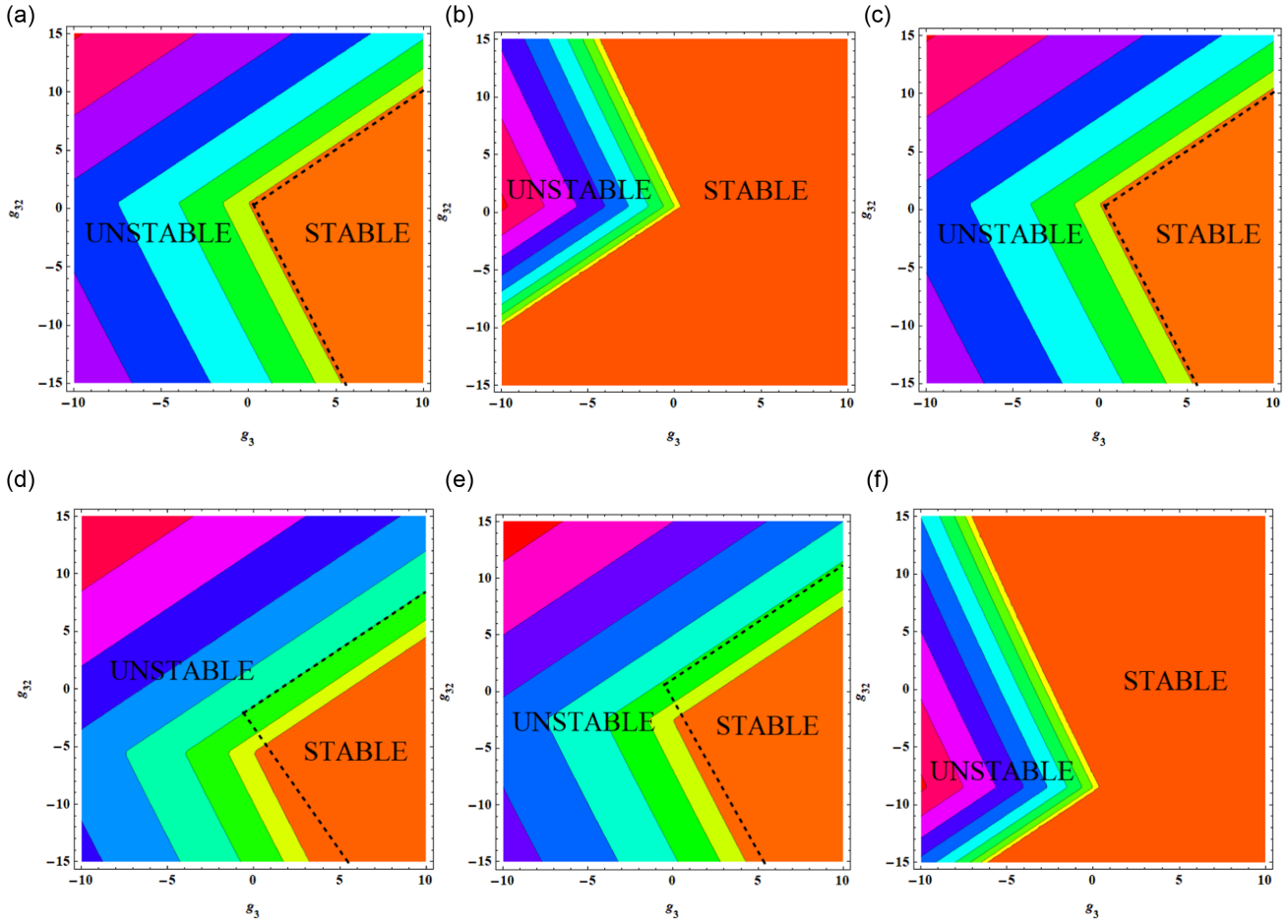

h_{32} plane when $p_{32} = 0$ are shown in Figure 3(a)–(c). As observed, the instability region contracts, and stable modes move into the immiscibility region as p_3 increases (assuming positive values signifying intra-species higher-order repulsion). The stability region widens, admitting extra unchanging modes, containing those with negative h_3 values, as intra-species higher-order collaborations become extra desirable, i.e., p_3 drops while captivating negative values. As a result, stronger intra-species repulsive forces are required to achieve stability with positive p_3 values. Accordingly, the ternary condensate is stabilized by intra-species higher-order attraction while it is destabilized by intra-species higher-order repulsion. To expand the instability band of three-body condensates, interspecies higher-order relations may be equally as significant as intra-component's higher-order relations. When intra-species higher-order dealings are striking ($p_3 < 0$), the instability zones in the h_3–h_{32} plane for diverse strengths of interspecies higher-order communications are shown in Figure 3(d)–(f). The line $h_{32} = 0$ in the diagram represents the symmetry of the stability region. Similar to $p_{32} = 0$, it denotes the lack of any remaining interspecies interactions. When the inter-components higher-order communications are attractive ($p_{32} < 0$), the stability zone moves to lower values of the interspecies three-body communication. The miscible area shifts to larger ideals of inter-component ternary-species relations for repulsive inter-component higher-order collaborations ($p_{32} > 0$). The behavior will be the same whether there are zero ($p_3 = 0$) or awful ($p_3 > 0$) intra-species higher-order interactions. As a result, stability is increased when the higher-order and ternary condensate connections are similar. The conclusions above imply additional requirements for instability and miscibility when higher-order interactions are not negligible. The swing along the h_{32} axis in Figure 3(d)–(f) is comparable to those figures' shortening of the constancy area. Figure 2(a)–(c) shows a shift along the h_3 axis. As a result, the higher-order relations move the instability illustration's position concerning the miscibility drawing in two different directions: to the right for rising p_3 and the left for lowering p_3, and to the other direction for changing p_{32}. Thus, we infer that the miscibility criterion would change to

Figure 3

Instability domain in the h_3 vs. h_{32} plane [(a)–(c)] when $p_{12} = p_{21} = p_{31} = p_{32} = p_{23} = 0$ (no interspecies higher-order interaction) and for innumerable power higher-order intra-species interactions $p_3 = 0, 6, -6$; and [(d)–(f)] when $p_3 = -6$ (intelligent intra-species higher-order interaction) and for innumerable strength of the interspecies higher-order communication $p_{32} = 0, -3, +3$, respectively. The red regions denote unchanging modes, whereas the rest of the realm signifies uneven modes, with the most unsteady in the black regions. Black dashed lines separate the miscible and immiscible zones

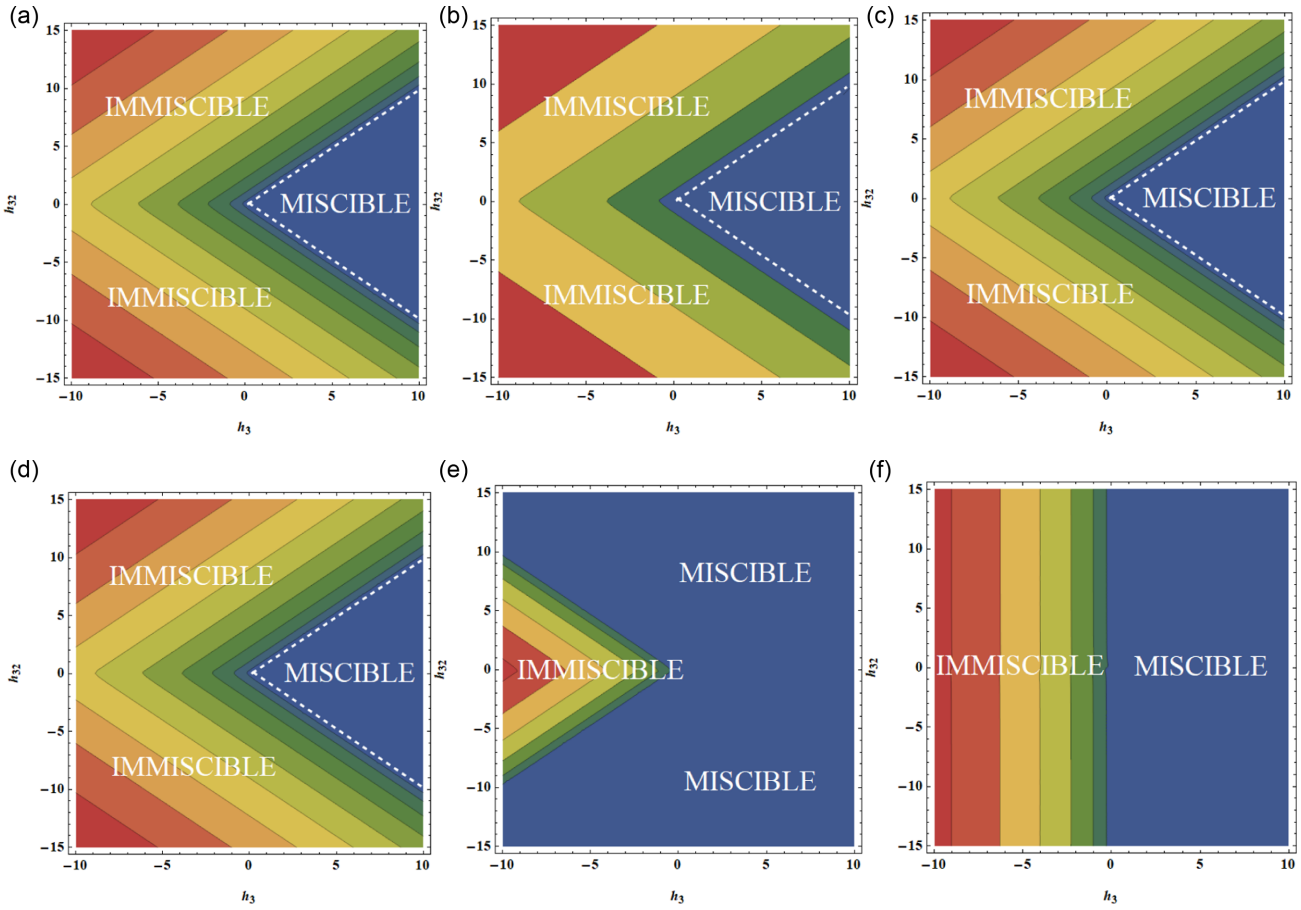

$$h_1h_2g_3 > h_{12}h_{21} \quad h_1h_2h_3 > h_{23}h_{32} \quad h_1h_2h_3 > h_{13}h_{31} \qquad (22)$$

Efficient communication power has a significant impact on MI. The wave number dependence would entail a very complex MI cascade situation. The supplementary enthusiastic modes increase the system's complexity when second-order MI develops. Effective interactions can improve or change a condensate mixture's immiscibility-miscibility, which can impact the instability excitation. In miscible states or phase-mixed, positive p_3 can, for instance, decrease repulsive three-body interaction and instability excitation. When p_3 and p_{32} are zero, the effective interaction strengths h_3 and h_{32} may change the instability excitation in miscible states. According to Ramakrishnan and Subramaniyan [10], these results qualitatively match the latter's exactly. Our understanding of the stability of BECs with three-body and higher-order interactions is deepened by the aforementioned findings. It is our hope that our study will encourage researchers to take this approach.

3.3. The p_3–p_{32} parameter plane

We may be attracted to carefully choosing higher-order connections when the ternary condensate communication powers are fixed on attaining or preventing MI. This section illustrates the three-component condensate instability zones for BECs with three-body repulsions in the higher-order communications region p_3 vs. p_{32}. Weaker and greater nauseas of interspecies three bodies are the two sorts of repulsions that concern us. We show the MI regions of the condensates in the p_3 versus p_{32} plane for severe interspecies ternary condensate revulsion (Figure 4(a)–(c)) and insignificant interspecies ternary condensates nausea (Figure 4(b)–(d)). Instability unchanging and unhinged areas are represented by the letters MS and MU, respectively. The undermining effect of repulsive intra-species' higher-order dealings is further proven here since bigger values of p_3 exist in the MU area, regardless of how intense the interspecies three-body repulsion is ($g_{12} = g_{21} = g_{23} = g_{32} = 4$) or how modest the repulsion is between the species ($g_{12} = g_{21} = g_{23} = g_{32} = 0.5$). The image also shows the influence of higher-order communications between species. See a superior MS area in the greater left corner of Figure 4(a) and (c) for additional evidence. Positive values of p_{32}, as can be shown, subsidize extra stability for strapping interspecies ternary condensates revulsion than for feeble interspecies ternary condensate repugnance. On the other hand, as the MS province becomes symmetric for minor interspecies ternary-component revulsion, positive and negative

Figure 4

Association of constancy areas when the inter-components revulsion is (a, c) intense, say $h_{23} = 4$, and (b, d) feeble with $h_{23} = 0.5$. The comparison is done in the p_3–p_{32} plane. We have motionless the values $g_1 = g_2 = g_3 = 1$ and $h_1 = h_2 = h_3 = 0.5$. Unchanging is MS, and unhinged is denoted as MU

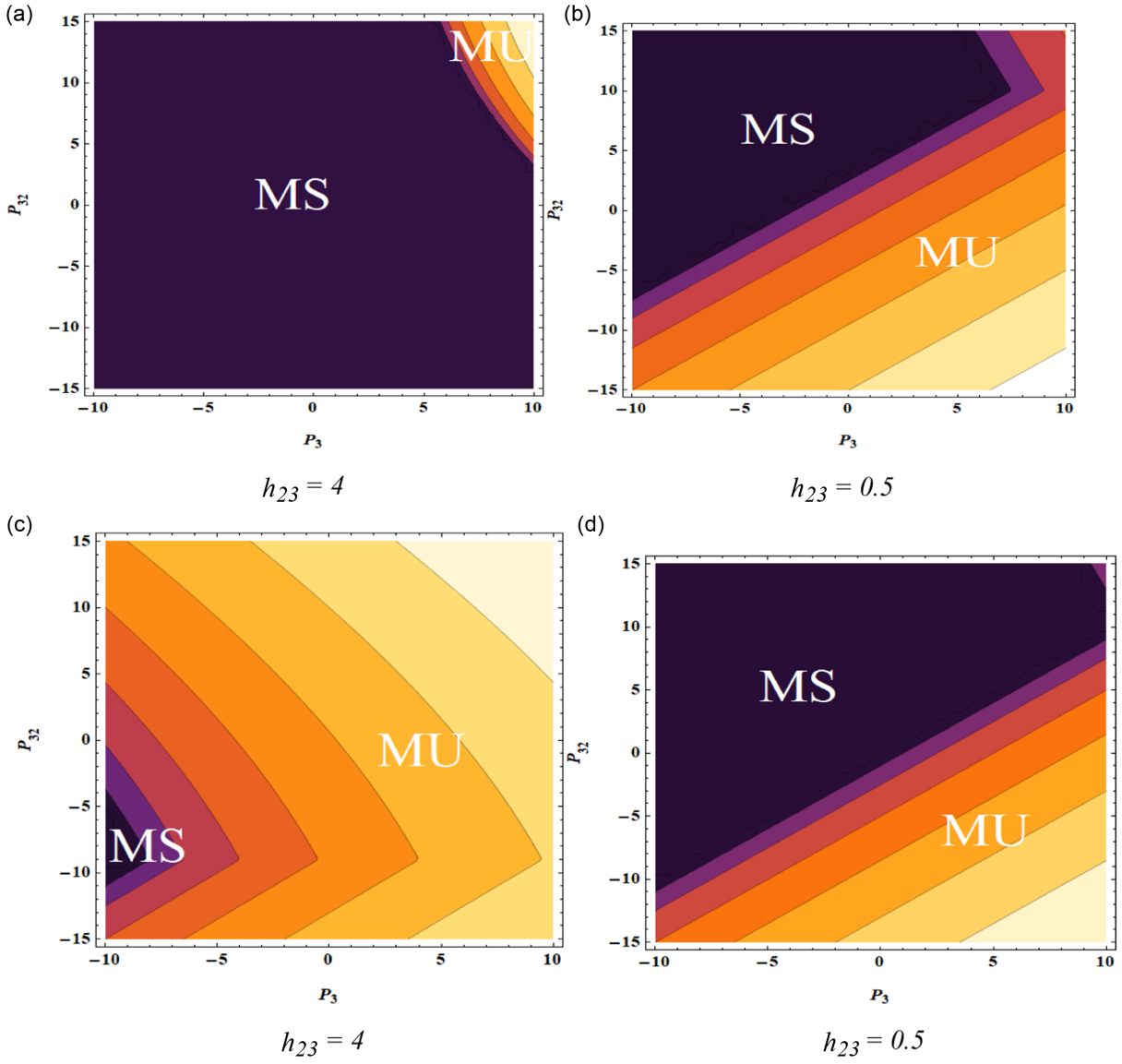

values of p_{32} virtually have a similar effect on the instability (see Figure 4(b) and (d)). The results obtained by Ramakrishnan and Subramaniyan [10] are completely in line with these findings in terms of quality. The aforementioned findings give us a better understanding of how stable BECs with three-body and higher-order interactions are. It is our hope that this investigation will serve as an inspiration to other experimentalists.

3.4. Higher-order effects

In this part, we examine the instability growth for a few modes relevant to the numerical computations as a function of Q. As shown in Figure 5(a)–(c), lower spatial frequencies are unchanging for intra-species higher-order fascination ($p_3 < 0$), whereas higher wave numbers are unhinged. The spectrum of unstable modes widened as we raised p_3. The three-dimensional instability growth outlines in Figure 5(a) and (b) display dual symmetric sidebands in the center of the excitation spatial vector plane Q. The MI gain thus permits the greatest 800 m^{-1}, which are reached at nil Q and $p_3 = 0$ correspondingly. The lobes disappear as the value of p_3 increases, as can be seen when comparing the two panels. The two-dimensional conspiracies along the line Q in Figures 5(c) and (d) show the standard one-component condensate MI gain profiles. For intra-species higher-order repulsion ($p_3 > 0$), smaller wave numbers become unchanging, whereas larger wave numbers become unhinged, as seen in Figure 5(e) and (f). When we raised g_{23} and g_{32}, the stable mode range grew. The 3D MI gain outline in Figure 5(e) displays a stability area in the excitation wave number plane Q. The instability sidebands were almost fully expanded in Figure 5(c), when the strength of interspecies ternary condensates revulsion proliferations. A valley-shaped MI gain profile is seen in Figure 5(g), and an upturned tapering hat is shown in Figure 5(h) in the associated two-dimensional plots along line Q. In both scenarios, the instability gain is at its extreme; larger spatial vector numbers are less stable than lesser ones. The combination of repulsive two-body contact, three-body interaction, and higher-order

Figure 5

Instability growth profile for numerous modes (a) $p_1 = p_2 = p_3 = 0$; $g_{12} = g_{21} = g_{32} = g_{23} = 4$, (b) $p_1 = p_2 = p_3 = 1$; $g_{12} = g_{21} = g_{32} = g_{23} = 4$, (e) $p_1 = p_2 = p_3 = 6$; $g_{12} = g_{21} = g_{32} = g_{23} = 4$, and (f) $p_1 = p_2 = p_3 = -6$; $g_{12} = g_{21} = g_{32} = g_{23} = 4$. The 2D designs (a), (c), (e), and (g) are the cross-sectional vision of 3D schemes (b), (d), (f), and (h), respectively. The impact of intra-species higher-order dealings in the instability gain sketch for revolting interspecies ternary condensates communications is exposed in sections (a)–(d). At stumpy wave numbers, two sidebands emerge, which narrow as the intensity of higher-order connections declines. Unchanging basin appears at lowest wave numbers in panels (e)–(h), where the intra-species higher-order exchanges are revolting. However, the interaction between ternary condensates across species is strengthened

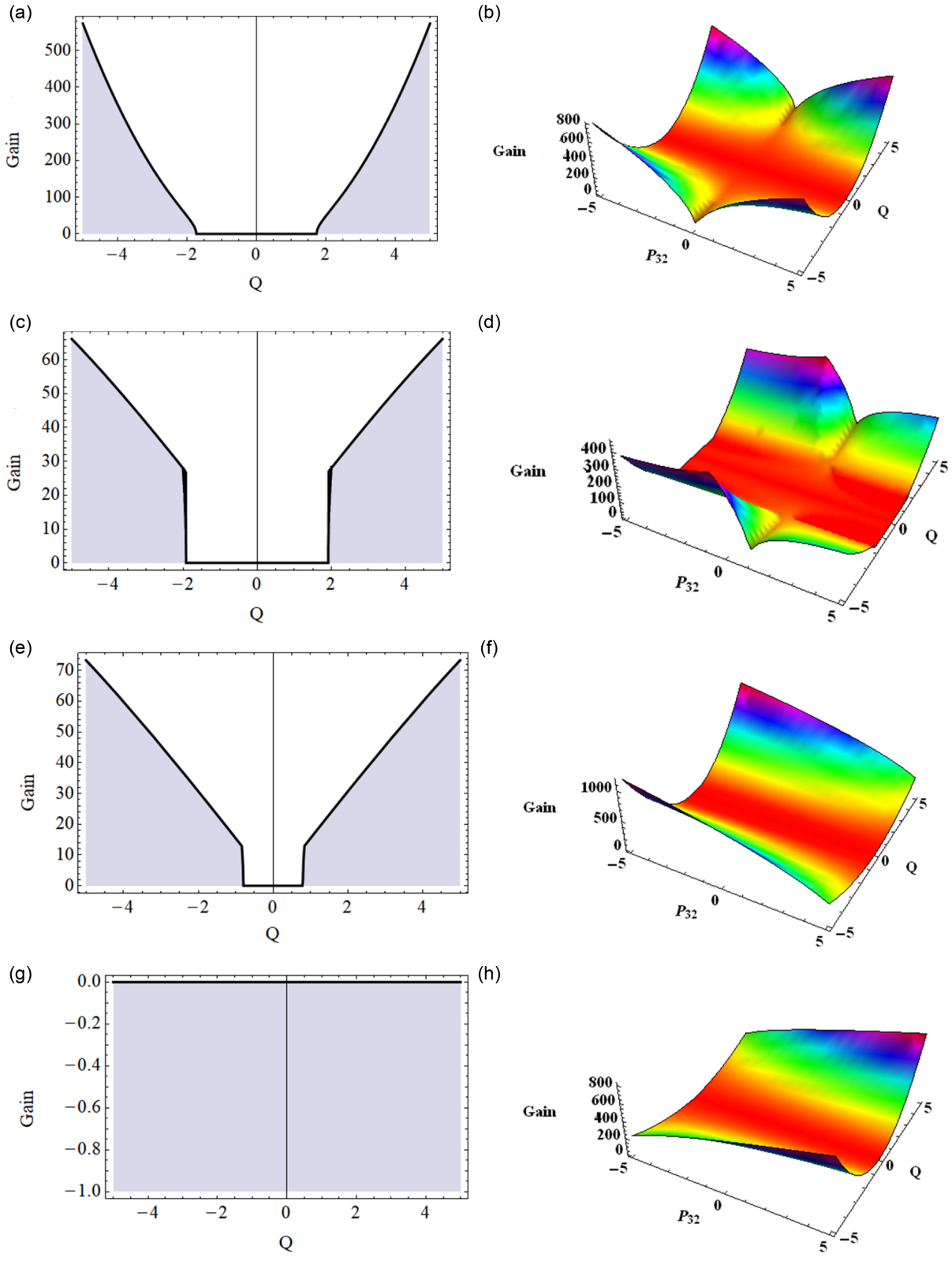

interaction leads to modulationally unstable regimes for the negative optical potential strength. The graphic illustrates the enhanced area within the region that corresponds to the negative domain of optical potential. Here, we note that adding the higher-order interaction three-body interaction to the repulsive condensate can amplify the system instability. This often contradicts the dynamics of instability in a basic nonlinear frame without a trap. The obtained results are qualitatively in good agreement with the outcome found by Ramakrishnan and Subramaniyan [10]. The aforementioned findings give us a better understanding of how stable BECs with three-body and higher-order interactions are. In this present work, encouragement can be used to test the other experimentalists in this direction.

4. Conclusion

Using an analytical approach, we have theoretically examined the MI of trapped BECs in the presence of three-body and higher-order interactions. It is observed that the three-body and higher-order interactions can play an important and prominent role in defining the stability of the BECs, particularly when examining the evolution of BECs in atomic waveguides with strong trap compression and on the surface of atomic chips. In these situations, there is a noticeable increase in the BEC density. With the aid of the LSA, we have analytically solved the modified GP equation. The ODEs for the time evolution of the perturbation parameters have been derived and analyzed. How the three-body and higher-order interactions affect the BEC dynamics through the LSA and without the need for a trapping potential were discussed. We found that the stable and unstable modes are equally divided due to shape-dependent confinement. The stability region in the plane similarly grows when we raise the strength of the h_3 parameter. These findings indicate that instability occurs, when the intra-species interaction is repulsive ($g_3 > 0$) and the interatomic interaction is attractive ($g_{32} < 0$). In addition, the higher-order relations move the MI diagram's position concerning the miscibility (MS) illustration in two different directions: to the right for rising p_3 and the left for lowering p_3 coefficient, and in the other direction for changing p_{32} coefficient. On the other hand, as the MS province becomes symmetric for minor interspecies ternary-component revulsion, positive and negative values of p_{32} virtually have a similar effect on the instability. The stable mode range grew when we raised the g_{23} and g_{32} coefficients. The 3D MI gain displays a stability area in the excitation wave number plane (Q). The instability sidebands almost fully expand when the strength of interspecies ternary condensates revulsion proliferations. More specifically, unstable modes arise from two-body interactions when there are no three-body or higher-order interactions. Conversely, the manifestation of MI is contingent upon the magnitude and orientation of three-body and higher-order interactions, which are under the control of the LSA technique.

Recommendations

The results showed that the optical fiber communication system is beneficial in addressing the issue of data transmission failure. It is therefore advised to use the current result, which is beneficial for both communication and other technologies. As a result, it was advised that tutors employ a range of instructional technology resources for instruction and evaluation.

Acknowledgement

The Department of Physics at Pondicherry University established a basic computing cluster facility, Matlab, and Maple. RS appreciates Pondicherry University for this. UGC vide F. No. 37-312/2009(SR) dated 12-01-2010; DSTFIST via SR/FST/PSII-021/2009 dated 13-08-2010. This work is devoted to our esteemed colleague, Prof. K. Porsezian (late), in recognition of his affection and encouragement during his lifetime.

Ethical Statement

This study does not contain any studies with human or animal subjects performed by any of the authors.

Conflicts of Interest

The authors declare that they have no conflicts of interest to this work.

Data Availability Statement

Data are available from the corresponding author upon reasonable request.

Author Contribution Statement

P. Mohanraj: Conceptualization, Methodology, Software, Writing – original draft. **R. Sivakumar:** Validation, Formal analysis, Investigation, Supervision. **Jayaprakash Kaliyamurthy:** Writing – review & editing, Visualization. **V. Kamalakar:** Writing – review & editing, Visualization. **J. Gajendiran:** Writing – review & editing, Visualization.

References

[1] Dalfovo, F., Giorgini, S., Pitaevskii, L. P., & Stringari, S. (1999). Theory of Bose-Einstein condensation in trapped gases. *Reviews of Modern Physics*, *71*(3), 463–512. https://doi.org/10.1103/RevModPhys.71.463

[2] Liu, Y. Y., Li, W. D., & Dai, W. S. (2021). Exactly solvable Gross–Pitaevskii type equations. *Journal of Physics Communications*, *5*(1), 015011. https://doi.org/10.1088/2399-6528/abda12

[3] Horvath, M. S., Thomas, R., Tiesinga, E., Deb, A. B., & Kjærgaard, N. (2017). Above-threshold scattering about a Feshbach resonance for ultracold atoms in an optical collider. *Nature Communications*, *8*(1), 452. https://doi.org/10.1038/s41467-017-00458-y

[4] Marchant, A. L., Billam, T. P., Wiles, T. P., Yu, M. M. H., Gardiner, S. A., & Cornish, S. L. (2013). Controlled formation and reflection of a bright solitary matter-wave. *Nature Communications*, *4*(1), 1865. https://doi.org/10.1038/ncomms2893

[5] Fragiadakis, D., & Roland, C. M. (2019). Intermolecular distance and density scaling of dynamics in molecular liquids. *The Journal of Chemical Physics*, *150*(20), 204501. https://doi.org/10.1063/1.5098455

[6] Sabari, S., Porsezian, K., & Murali, R. (2015). Modulational and oscillatory instabilities of Bose–Einstein condensates with two- and three-body interactions trapped in an optical lattice potential. *Physics Letters A*, *379*(4), 299–307. https://doi.org/10.1016/j.physleta.2013.12.047

[7] Dell'Anna, L., & Grava, S. (2021). Critical temperature in the BCS-BEC crossover with spin-orbit coupling. *Condensed Matter*, *6*(2), 16. https://doi.org/10.3390/condmat6020016

[8] Qi, X. Y., & Xue, J. K. (2012). Modulational instability of a modified Gross-Pitaevskii equation with higher-order nonlinearity. *Physical Review E—Statistical, Nonlinear, and*

Soft Matter Physics, *86*(1), 017601. https://doi.org/10.1103/PhysRevE.86.017601

[9] Ramakrishnan, T. T., Subramaniyan, S., & Porsezian, K. (2018). Stabilization of repulsive trapless Bose–Einstein condensates. *Journal of Physics B: Atomic, Molecular and Optical Physics*, *51*(16), 165202. https://doi.org/10.1088/1361-6455/aad038

[10] Ramakrishnan, T., & Subramaniyan, S. (2019). Stabilization of trapless Bose-Einstein condensates without any management. *Physics Letters A*, *383*(17), 2033–2038. https://doi.org/10.1016/j.physleta.2019.03.042

[11] Tran, B., Rautenberg, M., Gerken, M., Lippi, E., Zhu, B., Ulmanis, J., . . . , & Weidemüller, M. (2021). Fermions meet two bosons—The heteronuclear Efimov effect revisited. *Brazilian Journal of Physics*, *51*(2), 316–322. https://doi.org/10.1007/s13538-020-00811-5

[12] Flores-Calderón, R., Fujioka, J., & Espinosa-Cerón, A. (2021). Soliton dynamics of a high-density Bose-Einstein condensate subject to a time varying anharmonic trap. *Chaos, Solitons & Fractals*, *143*, 110580. https://doi.org/10.1016/j.chaos.2020.110580

[13] Ye, M., Tian, Y., Lin, J., Luo, Y., You, J., Hu, J., . . . , & Li, X. (2023). Universal quantum optimization with cold atoms in an optical cavity. *Physical Review Letters*, *131*(10), 103601. https://doi.org/10.1103/PhysRevLett.131.103601

[14] Golam Ali, S., Talukdar, B., & Saha, A. (2009). Effects of three-body atomic interaction and optical lattice on solitons in quasi-one-dimensional Bose-Einstein condensate. *Pramana*, *72*(2), 445–450. https://doi.org/10.1007/s12043-009-0039-2

[15] Raju, T. S., Panigrahi, P. K., & Porsezian, K. (2005). Modulational instability of two-component Bose-Einstein condensates in a quasi-one-dimensional geometry. *Physical Review A—Atomic, Molecular, and Optical Physics*, *71*(3), 035601. https://doi.org/10.1103/PhysRevA.71.035601

[16] Mithun, T., & Kasamatsu, K. (2019). Modulation instability associated nonlinear dynamics of spin–orbit coupled Bose–Einstein condensates. *Journal of Physics B: Atomic, Molecular and Optical Physics*, *52*(4), 045301. https://doi.org/10.1088/1361-6455/aafbdd

[17] Sabari, S., Lekeufack, O. T., Yamgoue, S. B., Tamilthiruvalluvar, R., & Radha, R. (2022). Role of higher-order interactions on the modulational instability of Bose-Einstein condensate trapped in a periodic optical lattice. *International Journal of Theoretical Physics*, *61*(8), 222. https://doi.org/10.1007/s10773-022-05204-9

[18] Subramaniyan, S., Lekeufack, O. T., Radha, R., & Kofane, T. C. (2020). Interplay of three-body and higher-order interactions on the modulational instability of Bose–Einstein condensate. *Journal of the Optical Society of America B*, *37*(11), A54–A61. https://doi.org/10.1364/JOSAB.395007

[19] Agrawal, G. P. (1995). *Nonlinear fiber optics* (2nd ed.). USA: Academic Press.

[20] Tabi, C. B., Otlaadisa, P., & Kofané, T. C. (2022). Modulation instability of two-dimensional Bose-Einstein condensates with helicoidal and a mixture of Rashba-Dresselhaus spin-orbit couplings. *Physics Letters A*, *449*, 128334. https://doi.org/10.1016/j.physleta.2022.128334

[21] Chen, J., & Zeng, J. (2020). One-dimensional localized modes of spin-orbit-coupled Bose-Einstein condensates with spatially periodic modulated atom-atom interactions: Nonlinear lattices. *Communications in Nonlinear Science and Numerical Simulation*, *85*, 105217. https://doi.org/10.1016/j.cnsns.2020.105217

[22] Watabe, S. (2020). Strong connection between single-particle and density excitations in Bose–Einstein condensates. *New Journal of Physics*, *22*(10), 103010. https://doi.org/10.1088/1367-2630/abb2b6

[23] He, J., & Lin, J. (2023). Stationary and moving bright solitons in Bose–Einstein condensates with spin–orbit coupling in a Zeeman field. *New Journal of Physics*, *25*(9), 093041. https://doi.org/10.1088/1367-2630/acf8eb

[24] Zhou, Y., Meng, H., Zhang, J., Li, X., Ren, X., Wan, X., . . . , & Shi, Y. (2021). Stability analysis on dark solitons in quasi-1D Bose–Einstein condensate with three-body interactions. *Scientific Reports*, *11*(1), 11382. https://doi.org/10.1038/s41598-021-90814-2

[25] Mohanraj, P., & Sivakumar, R. (2023). Effects of residual nonlinearities on the modulational instability of three-component Bose–Einstein condensates. *Physica Scripta*, *98*(8), 085239. https://doi.org/10.1088/1402-4896/ace854

[26] Kartashov, Y. V., Malomed, B. A., Tarruell, L., & Torner, L. (2018). Three-dimensional droplets of swirling superfluids. *Physical Review A*, *98*(1), 013612. https://doi.org/10.1103/PhysRevA.98.013612

[27] Hammond, A., Lavoine, L., & Bourdel, T. (2022). Tunable three-body interactions in driven two-component Bose-Einstein condensates. *Physical Review Letters*, *128*(8), 083401. https://doi.org/10.1103/PhysRevLett.128.083401

[28] Levinsen, J., Parish, M. M., & Bruun, G. M. (2015). Impurity in a Bose-Einstein condensate and the Efimov effect. *Physical Review Letters*, *115*(12), 125302. https://doi.org/10.1103/PhysRevLett.115.125302

[29] Abdullaev, F. K., Gammal, A., Tomio, L., & Frederico, T. (2001). Stability of trapped Bose-Einstein condensates. *Physical Review A*, *63*(4), 043604. https://doi.org/10.1103/PhysRevA.63.043604

How to Cite: Mohanraj, P., Sivakumar, R., Kaliyamurthy, J., Kamalakar, V., & Gajendiran, J. (2025). Role of Higher-Order Scattering Coefficient and Residual Nonlinearities on Instability Criteria in Three-Body Bose-Einstein Condensates. *Journal of Optics and Photonics Research*, *2*(4), 191–202. https://doi.org/10.47852/bonviewJOPR42022330

Appendix

The following lists the non-zero matrix entries.

$$M_{11} = \omega - a_1^2 g_1 - 2a_1^4 h_1 + Q^2 a_1^2 P_1 - Q^2 \beta_1;$$

$$M_{12} = M_{22} = -a_1 a_2 g_{12} - 2a_1 a_2^3 h_{12} + Q^2 a_1 a_2 P_{12};$$

$$M_{13} = M_{23} = -a_1 a_3 g_{13} - 2a_1 a_3^3 h_{13} + Q^2 a_1 a_3 P_{13};$$

$$M_{14} = M_{21} = -a_1^2 g_1 - 2a_1^4 h_1 + Q^2 a_1^2 P_1;$$

$$M_{15} = M_{25} = -a_1 a_2 g_{12} - 2a_1 a_2^3 h_{12} + Q^2 a_1 a_2 P_{12};$$

$$M_{16} = M_{26} = -a_1 a_3 g_{13} - 2a_1 a_3^3 h_{13} + Q^2 a_1 a_3 P_{13};$$

$$M_{24} = -\omega - a_1^2 g_1 - 2a_1^4 h_1 + Q^2 a_1^2 P_1 - Q^2 \beta_1;$$

$$M_{31} = M_{41} = -a_1 a_2 g_{21} - 2a_1^3 a_2 h_{21} + Q^2 a_1 a_2 P_{21};$$

$$M_{32} = \omega - a_2^2 g_2 - 2a_2^4 h_2 + Q^2 a_2^2 P_2 - Q^2 \beta_2;$$

$$M_{33} = M_{43} = -a_2 a_3 g_{23} - 2a_2 a_3^3 h_{23} + Q^2 a_2 a_3 P_{23};$$

$$M_{34} = M_{44} = -a_1 a_2 g_{21} - 2a_1^3 a_2 h_{21} + Q^2 a_1 a_2 P_{21};$$

$$M_{35} = M_{42} = -a_2^2 g_2 - 2a_2^4 h_2 + Q^2 a_2^2 P_2;$$

$$M_{45} = -\omega - a_2^2 g_2 - 2a_2^4 h_2 + Q^2 a_2^2 P_2 - Q^2 \beta_2;$$

$$M_{36} = M_{46} = -a_2 a_3 g_{23} - 2a_2 a_3^3 h_{23} + Q^2 a_2 a_3 P_{23};$$

$$M_{51} = M_{61} = -a_1 a_3 g_{31} - 2a_1^3 a_3 h_{31} + Q^2 a_1 a_3 P_{31};$$

$$M_{52} = M_{62} = -a_2 a_3 g_{32} - 2a_2^3 a_3 h_{32} + Q^2 a_2 a_3 P_{32};$$

$$M_{53} = \omega - a_3^2 g_3 - 2a_3^4 h_3 + Q^2 a_3^2 P_3 - Q^2 \beta_3;$$

$$M_{54} = M_{64} = -a_1 a_3 g_{31} - 2a_1^3 a_3 h_{31} + Q^2 a_1 a_3 P_{31};$$

$$M_{55} = M_{65} = -a_2 a_3 g_{32} - 2a_2^3 a_3 h_{32} + Q^2 a_2 a_3 P_{32};$$

$$M_{66} = -\omega - a_3^2 g_3 - 2a_3^4 h_3 + Q^2 a_3^2 P_3 - Q^2 \beta_3;$$

$$M_{56} = M_{63} = -a_3^2 g_3 - 2a_3^4 h_3 + Q^2 a_3^2 P_3;$$